Nanoscale Research Letters

NANO EXPRESS Open Access

Effects of Post Annealing on Electrical Performance of Polycrystalline Ga_2O_3 Photodetector on Sapphire

Haodong Hu[1†], Yuchen Liu[1†], Genquan Han[1*], Cizhe Fang[1], Yanfang Zhang[2], Huan Liu[1], Yibo Wang[1], Yan Liu[1], Jiandong Ye[2] and Yue Hao[1]

Abstract

Effects of post annealing on the physical and electrical properties of solar-blind polycrystalline gallium oxide (Ga_2O_3) ultraviolet photodetectors on the sapphire substrate are investigated. The grain size of poly-Ga_2O_3 becomes larger with the post annealing temperature (PAT) increasing from 800 °C to 1000 °C, but it gets smaller with further raising PAT to 1100 °C. A blue shift is observed at the absorption edge of the transmittance spectra of Ga_2O_3 on sapphire as increasing PAT, due to the incorporation of Al from the sapphire substrate into Ga_2O_3 to form $(Al_xGa_{1-x})_2O_3$. The high-resolution X-ray diffraction and transmittance spectra measurement indicate that the substitutional Al composition and bandgap of $(Al_xGa_{1-x})_2O_3$ annealed at 1100 °C can be above 0.30 and 5.10 eV, respectively. The R_{max} of the sample annealed at 1000 °C increases about 500% compared to the as-deposited device, and the sample annealed at 1000 °C has short rise time and decay time of 0.148 s and 0.067 s, respectively. This work may pave a way for the fabrication of poly-Ga_2O_3 ultraviolet photodetector and find a method to improve responsivity and speed of response.

Keywords: Gallium oxide (Ga_2O_3), Post annealing, Solar-blind, Ultraviolet, Photodetector

Background

Deep ultraviolet (DUV) solar-blind photodetectors have a wide range of applications such as monitoring ozone holes and detecting flames with the inherent advantage of strong anti-interference ability [1]. Compared with traditional semiconductor materials like silicon and germanium, wide bandgap semiconductor materials are considered to be ideal materials for solar-blind photodetectors which have better selectivity for ultraviolet light and better adaptability in harsh environments [2]. Lots of researchers have been focused on AlGaN, MgZnO, and Ga_2O_3 DUV solar-blind photodetectors [2–4]. Ga_2O_3 attracts great attention due to its superior optical properties, chemical stability, and high strength with a bandgap of 4.8 eV, which is a promising material for solar-blind photodetectors [5–13]. Ga_2O_3 thin films have been obtained on foreign substrates by molecular beam epitaxy (MBE) [5, 6], radio-frequency magnetron sputtering (RFMS) [7], pulsed laser deposition (PLD) [8, 9], atomic layer deposition (ALD) [10], halide vapor phase epitaxy (HVPE) [11], metal-organic chemical vapor deposition (MOCVD) [12], and sol-gel method [13]. Among these methods, RFMS deposition has been widely used to fabricate various films due to its advantages of easy controllability, high efficiency, harmless, and low cost. Therefore, we used this method to grow Ga_2O_3 thin films for DUV solar-blind photodetectors.

In this work, poly-Ga_2O_3 solar-blind photodetectors were fabricated on the sapphire substrate. It is demonstrated that the Al atoms are incorporated from the sapphire substrate into Ga_2O_3 to form $(Al_xGa_{1-x})_2O_3$ after post thermal annealing. The structural properties,

* Correspondence: hangenquan@gmail.com; gqhan@xidian.edu.cn
Haodong Hu and Yuchen Liu are equal contributors.
[1]State Key Discipline Laboratory of Wide Band Gap Semiconductor Technology, School of Microelectronics, Xidian University, Xi'an 710071, China
Full list of author information is available at the end of the article

substitutional Al composition x, optical properties, and photodetector performance of poly-$(Al_xGa_{1-x})_2O_3$ films with different post annealing temperatures (PATs) were investigated.

Method

In this experiment, poly-Ga_2O_3 thin films were grown on single-polished (0006)-oriented sapphire substrates by RFMS at 600 °C with the sputtering power of 120 W. The working pressure was kept constant at 5 mTorr and the flow of argon was 20 sccm throughout the deposition. The thickness of the films deposited on sapphire was measured to be around 164 nm. After the deposition, post thermal annealing was carried out in an air atmosphere for 1 h at 800 °C, 900 °C, 1000 °C, and 1100 °C. After annealing, the samples were cooled to room temperature with a speed of 100 °C/min. The 30 nm Ti and 80 nm Ni were then deposited by magnetron sputtering as an electrode. After the interdigital electrode patterning and etching, the metallic contacts on Ga_2O_3 were formed by the rapid thermal annealing at 470 °C in a nitrogen atmosphere [14]. The fabricated poly-Ga_2O_3 solar-blind photodetectors have metal-semiconductor-metal (MSM) interdigital electrodes as shown in Fig. 1. The length, width, and space between the fingers were 500 μm, 6 μm, and 15 μm, respectively, and the total length of the fingers is 1.8 cm.

Results and Discussion

The structural properties of the Ga_2O_3 films were investigated by high-resolution X-ray diffraction (HRXRD). Figure 2 presents the HRXRD curves for the samples that as-deposited and annealed at different temperatures. Peaks corresponding to $(\bar{2}01)$, (400), (111), $(\bar{4}02)$, (600), (510), and $(\bar{6}03)$ planes of β-Ga_2O_3 crystals [15] reveal that the Ga_2O_3 film consists of monoclinic β-Ga_2O_3 polycrystalline with random orientation. The as-deposited sample exhibits a higher peak intensity for the (400) plane compared to the other planes. The PAT leads to the improvement of the intensities of $(\bar{2}01)$, (400), $(\bar{4}02)$, and $(\bar{6}03)$ planes.

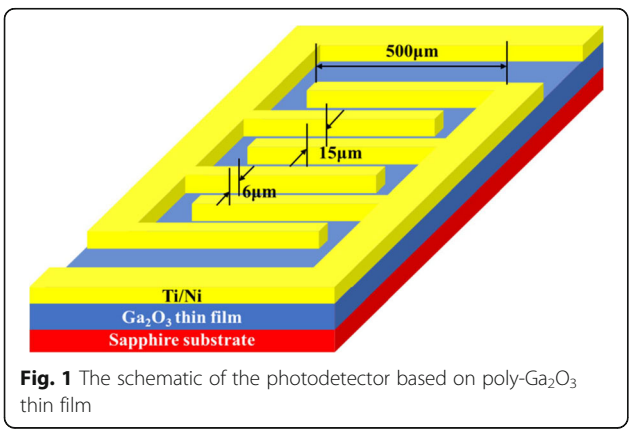

Fig. 1 The schematic of the photodetector based on poly-Ga_2O_3 thin film

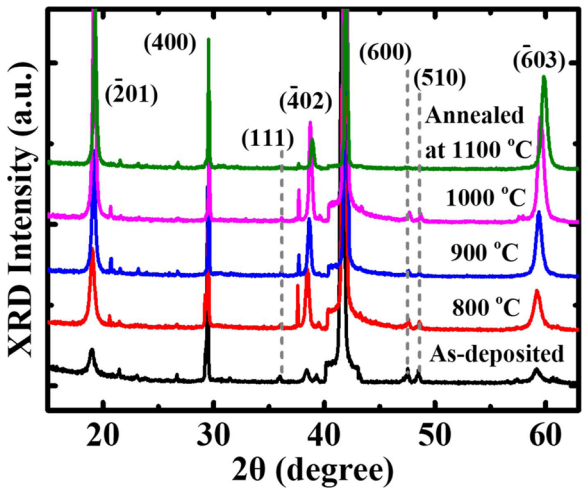

Fig. 2 The XRD peaks of the samples without and with post thermal annealing at different temperatures

Figure 3a and b focus on the HRXRD peaks for $(\bar{2}01)$ and $(\bar{6}03)$ planes, respectively. The full width at half maximum (FWHM) of the peak was used to calculate the grain size by solving the Debye-Scherrer formula [16] to evaluate the dependence of the crystalline quality of Ga_2O_3 films on PAT. It can be seen from Table 1 that higher annealing temperature yields larger grain size as PAT increases from 800 °C to 1000 °C, but the grain size decreases slightly at the PAT of 1100 °C. The diffusion of Al from the Al_2O_3 substrates into Ga_2O_3 films underwent a PAT above 1000 °C has been widely observed [17–19]. As shown in Fig. 3c, the peaks of HRXRD shifting to the higher diffraction angle is due to that Al from the sapphire substrate diffuses into Ga_2O_3 film to form $(Al_xGa_{1-x})_2O_3$ after annealing.

Based on the Bragg's law, the plane spacing d of $(\bar{2}01)$ and $(\bar{6}03)$ planes of $(Al_xGa_{1-x})_2O_3$ are calculated and shown in Fig. 3d, respectively. According to Ref. [20], the lattice parameters can be calculated by $a = (12.21 - 0.42x)$ Å, $b = (3.04 - 0.13x)$ Å, $c = (5.81 - 0.17x)$ Å, $\beta = (103.87 + 0.31x)°$. The d of $(\bar{6}03)$ is expressed as [21]

$$\frac{1}{d^2} = \frac{h^2}{a^2 \sin^2\beta} + \frac{k^2}{b^2} + \frac{l^2}{c^2 \sin^2\beta} - \frac{2hl\cos\beta}{ac\sin^2\beta}, \quad (1)$$

where $h = -6$, $k = 0$, and $l = 3$. Based on the values in Fig. 3d, the x of poly-$(Al_xGa_{1-x})_2O_3$ can be achieved. The bandgap E_g of $(Al_xGa_{1-x})_2O_3$ can be calculated by

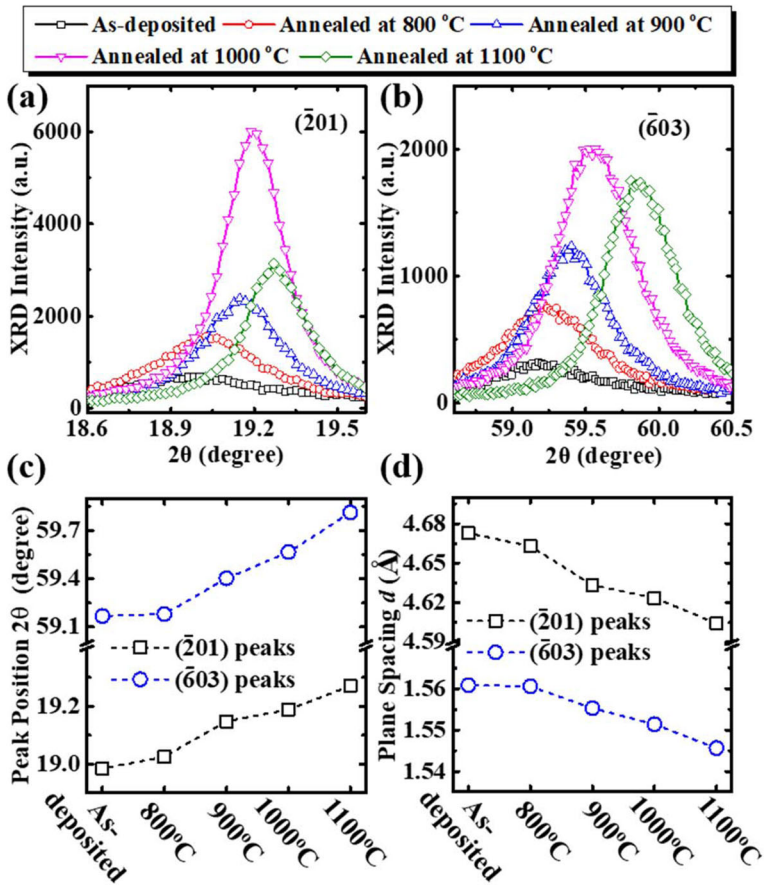

Fig. 3 The XRD peaks of **a** ($\bar{2}$01) plane and **b** ($\bar{6}$03) plane of the samples before and after annealing. **c** peak position and **d** plane spacing of ($\bar{2}$01) and ($\bar{6}$03) planes

$$E_g(x) = (1-x)E_g[Ga_2O_3] + xE_g[Al_2O_3] - nx(1-x), \quad (2)$$

where E_g [Ga_2O_3] = 4.65 eV, E_g [Al_2O_3] = 7.24 eV, n = 1.87 eV [22]. The calculated x and E_g values of the poly-$(Al_xGa_{1-x})_2O_3$ are shown in Table 2. An x value above 0.30 is achieved in the sample after a PAT at 1100 °C.

Atomic force microscope (AFM) images in Fig. 4 show that the surface root-mean-square (RMS) roughness values of the as-deposited film and the samples annealed at 800 °C and 900 °C are 3.62 nm, 10.1 nm, and 14.1 nm, respectively. The recrystallization caused by the high PAT results in a larger grain size, which can be additionally confirmed by a rougher surface.

Table 1 The grain size of polycrystalline films at different annealing temperatures

Temperature (℃)	FWHM (°)	Grain size (nm)
As-deposited	0.49135	15.99
800	0.47789	16.22
900	0.37031	20.93
1000	0.28513	27.18
1100	0.29602	26.18

The values of E_g of the $(Al_xGa_{1-x})_2O_3$ thin films before and after annealing were characterized by measuring the transmittance spectra. As shown in Fig. 5a, the annealed samples have a blue shift at the absorption edge compared to the as-deposited one. A shorter λ is acquired with the increase of PAT, due to the incorporation of Al. The Ga_2O_3 samples have a very low transmittance even in the visible range, which might be due to the nonradiative complex absorption induced by the defects in the materials. The absorption coefficient α of the films is calculated by [23, 24]

Table 2 Comparison of the calculated Al content and E_g of poly-$(Al_xGa_{1-x})_2O_3$ after thermal annealing according to HRXRD in Fig. 3 and experimental results of transmittance spectra

	800 °C	900 °C	1000 °C	1100 °C
Substitutional Al composition	0.02	0.14	0.22	0.35
Calculated E_g	4.67 eV	4.79 eV	4.90 eV	5.13 eV
Experimental E_g	4.72 eV	4.78 eV	4.81 eV	5.10 eV

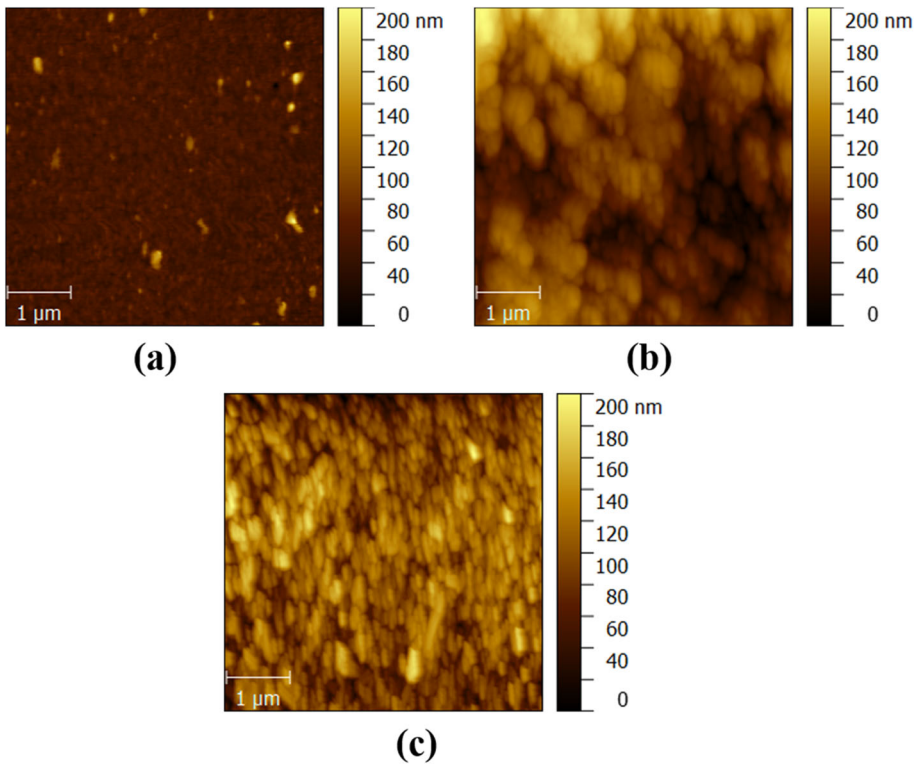

Fig. 4 AFM images of **a** as-deposited poly-Ga_2O_3 on sapphire, **b** samples annealed at 800 °C, and **c** 900 °C

$$\alpha = (1/t)\ \ln\left[(1-r)^2/T\right], \tag{3}$$

where T is the transmittance, r is the reflectance, and t is the film thickness. The relation between absorption coefficient α and incident photon energy hν follows a power law of the form

$$(\alpha h\nu) = B\left(h\nu - E_g\right)^{1/2}, \tag{4}$$

where B is the absorption edge width parameter [23]. By using these formulas, the relationship between hν and $(\alpha h\nu)^2$ can be obtained as shown in Fig. 5b. By extrapolating the linear regions of the plot to the horizontal axis, the E_g values of the samples are evaluated as 4.65 eV, 4.72 eV, 4.78 eV, 4.81 eV, and 5.10 eV. As shown in Table 2, the experimental E_g values of the samples are consistent with those calculated based on the HRXRD results.

To investigate the responsivity R and photocurrent I_{photo} of poly-$(Al_xGa_{1-x})_2O_3$ photodetectors, optical measurements varied different illumination λ from 220 to 300 nm with a P_{light} of 0.5 mW/cm^2. The R is calculated by

$$R = \left(I_{photo} - I_{dark}\right)/\left(P_{light}S\right), \tag{5}$$

where I_{dark} is the dark current and S is the effective illuminated area. Figure 6 shows a visible blue shift in maximum R of the annealed samples compared to the as-deposited film. This proves that a larger E_g of polycrystalline samples has been obtained after annealing with the diffusion of Al from the sapphire substrate into Ga_2O_3 to form $(Al_xGa_{1-x})_2O_3$. The R_{max} of the device annealed at 1100 °C is 35 μA/W, which is smaller than the 0.037 A/W, 0.903 A/W, and 1.13 mA/W those were grown by MBE [5], PLD [25], and sol-gel method [26], respectively, due to the fact that the poly-Ga_2O_3 has a low transmittance, as shown in Fig. 5a. But compared to the as-deposited device, the R_{max} of the device annealed at 1000 °C increases by about 500%. It is noted that R of devices decreases at wavelength shorter than that at R_{max}, similar to that in [27]. This could be due to the energy loss occurs during the relaxation process of carriers in case of photon energy above E_g of materials. R_{max} increasing with the PAT rising from 800 °C to 1000 °C is attributed to the increased grain size of the film.

Figure 7 shows the photocurrent I_{photo}, dark current I_{dark}, and PDCR versus bias voltage V_{bias} for the photodetectors under the illumination intensity of 0.5 mW/cm^2 and λ of 254 nm. As shown in Fig. 7a, I_{photo} increases almost linearly with the V_{bias}. Furthermore, as PAT raises from 800 °C to 1000 °C, photodetectors gain a larger I_{photo}. But the I_{photo} of the device annealed at 1100 °C is lower than that of the as-deposited sample, due to the energy of the photon is less than bangap of

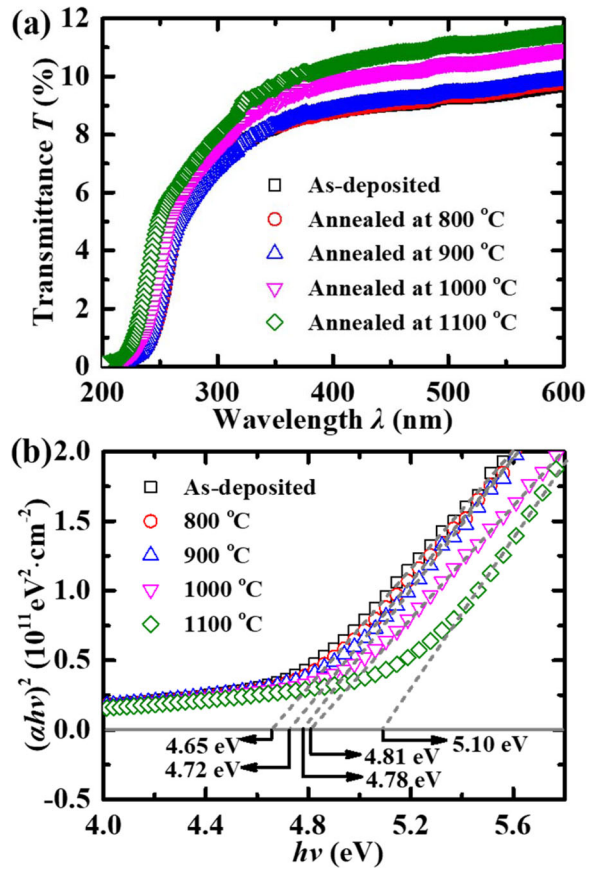

Fig. 5 **a** Transmittance spectra of as-deposited and annealed poly-$(Al_xGa_{1-x})_2O_3$ samples **b** $(\alpha h\nu)^2$ vs. $h\nu$ curves for poly-Ga_2O_3 samples. The extrapolation of the linear regions to the horizontal axis estimates the E_g values

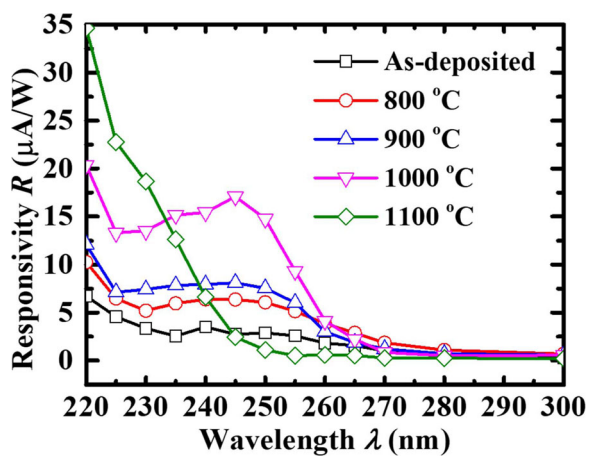

Fig. 6 R versus illumination optical λ for the poly-$(Al_xGa_{1-x})_2O_3$ photodetectors at V_{bias} of 5 V

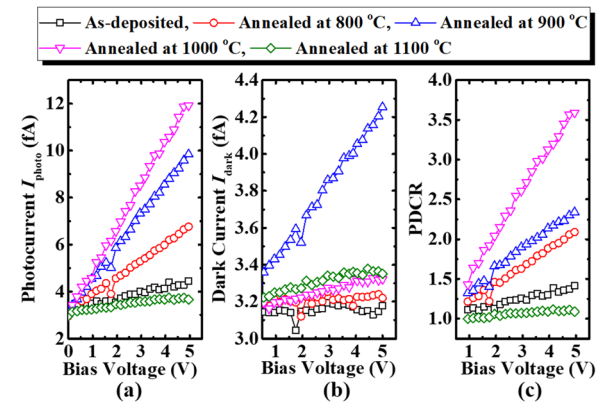

Fig. 7 **a** I_{photo}-V_{bias}, **b** I_{dark}-V_{bias}, and **c** PDCR characteristics of the as-deposited poly-$(Al_xGa_{1-x})_2O_3$ film and the samples annealed at different temperatures under the illumination intensity of 0.5 mW/cm^2 and λ of 254 nm

the sample annealed at 1100 °C, which cannot generate photo-carriers. The annealed samples show a higher I_{dark} than the as-deposited sample, as depicted in Fig. 7b. It is speculated that the recrystallization enhances the conductivity of poly-Ga_2O_3, resulting in the enhancement of both I_{photo} and I_{dark} of the photodetectors, and the

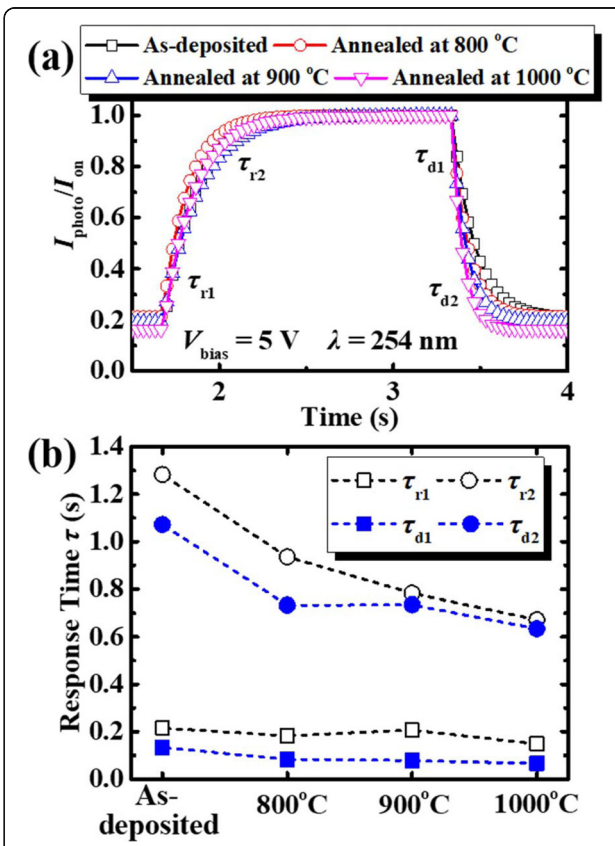

Fig. 8 **a** Time-dependence of photoresponse characteristics **b** rise and decay time

Table 3 The rise time and decay time of UV photodetectors without post annealing and after the annealing at different temperatures

Temperature (℃)	τ_{r1} (s)	τ_{r2} (s)	τ_{d1} (s)	τ_{d2} (s)
As-deposited	0.215	1.283	0.133	1.072
800	0.183	0.936	0.083	0.733
900	0.207	0.783	0.078	0.735
1000	0.148	0.672	0.067	0.634

PDCR of the sample with a PAT of 1000 °C is higher than those of the other samples. It can be noted that the dark current of the sample annealed at 900 °C is larger than others, which may be ascribed to the increased carriers with the PAT increasing, but with the PAT further increasing, interdiffusion of the Al and Ga takes place on a sapphire substrate, thus destroying the conductivity of the film [17].

The photoresponse characteristics of the photodetectors are depicted in Fig. 8a. An illumination with λ of 254 nm was used during the measurements. The P_{light}, V_{bias}, and period were 0.5 mW/cm^2, 5 V, and 5 s, respectively. There are two procedures of rising and decaying processes: fast-response and slow-response. Generally, the fast-response component can be attributed to the rapid change of carrier concentration as soon as the light is turned on/off [28], while the photogenerated carriers might be trapped by the defect levels in the bandgap, which could delay the carrier collection during the UV illumination and recombination as the light was turned off, resulting in the slow-response component. For a quantitative comparison study of the photodetector annealed at the different temperatures, the rise and decay processes can be fitted with a biexponential relaxation equation of the following type [29]:

$$I = I_0 + Ce^{-t/\tau_1} + De^{-t/\tau_2}, \quad (6)$$

where I_0 is the steady-state photocurrent, t is the time, C and D are the constant, τ_1 and τ_2 are two relaxation time constants. The rise time τ_{r1} and τ_{r2} correspond to the fast-response and the slow-response, respectively, and the decay time τ_{d1} and τ_{d2} of each photodetector are calculated, as shown in Table 3. It is clearly seen that the response time decreases after the annealing process. The rise time τ_{r1} is reduced from 0.215 s to 0.148 s, and the decay time τ_{d1} is reduced from 0.133 to 0.067 s. It is ascribed to the fact that the annealing process reduces the oxygen vacancies concentration in the poly-Ga_2O_3 film [28]. The direct transition becomes the main source of photo-generated unbalanced carriers, thereby the fast-response time decreases. The decay time τ_{d2} decreases from 1.072 to 0.634 s, indicating that there are fewer oxygen vacancies and other defects in the annealed samples as well, due to the time constant of the transient decay is generally governed by these traps. Further, the increased grain size with PAT can reduce the photocarriers transportation time, improving the relaxation time properties of the devices.

Table 4 shows the comparison of the I_{dark}, rise time (τ_r), and decay time (τ_d) of solar-blind photodetectors based on β-, α-, and ε-Ga_2O_3 thin films synthesized by RFMS [30] and other techniques [2, 6, 26, 31–34]. As seen, the device has both low dark current and fast response time is difficult, but the photodetector we fabricated presents the low dark current and fast response time.

Conclusions

In summary, we deposited poly-Ga_2O_3 thin film by magnetron sputtering on the c-plane sapphire substrate with post thermal annealing under different temperature; then, the ultraviolet poly-Ga_2O_3 photodetector was fabricated. Compared to the as-deposited Ga_2O_3 thin film, the annealed samples possess a larger grain size and a wider bandgap due to the recrystallization and the diffusion of the Al into Ga_2O_3. The R_{max} of the device annealed at 1000 °C increases about 500% compared to the as-deposited device, and the sample annealed at 1000 °C shows a low dark current of 0.0033 nA under

Table 4 The comparison of the I_{dark}, rise time (τ_r) and decay time (τ_d) of solar-blind photodetectors based on β-, α-, and ε-Ga_2O_3 thin films synthesized by different techniques

Material	Method	I_{dark} (nA)	Rise time τ_r (s)	Decay time τ_d (s)	Ref.
Poly-Ga_2O_3	RFMS	0.0033 (5 V)	0.148/0.672	0.067/0.634	This work
β-Ga_2O_3	RFMS	0.11 (10 V)	0.31/1.52	0.05/0.91	[30]
β-Ga_2O_3	Laser MBE	80 (10 V)	0.86	1.02/16.61	[6]
β-Ga_2O_3	MBE	4 (20 V)	3.33	0.4	[31]
β-Ga_2O_3	PLD	430 (20 V)	0.87/10.81	0.54/13.98	[2]
β-Ga_2O_3	MOCVD	34 (10 V)	0.48	0.18	[32]
β-Ga_2O_3	Sol-gel	0.758 (30 V)	0.1/0.18	0.1/1.85	[26]
α-Ga_2O_3	MOCVD	8.1×10^{-5} (12 V)	Not given	0.042	[33]
ε-Ga_2O_3	MOCVD	0.037 (200 V)	2.5	0.4/2.6	[34]

the bias of 5 V. Furthermore, the solar-blind photodetector fabricated on the film annealed at 1000 °C shows fast response time, with a rise and decay time of 0.148 s and 0.067 s, respectively. These results are useful to fabricate the DUV photodetectors with low dark current and fast response time.

Abbreviations

Ga_2O_3: Gallium oxide; PAT: Post annealing temperature; DUV: Deep ultraviolet; MBE: Molecular beam epitaxy; RFMS: Radio-frequency magnetron sputtering; PLD: Pulsed laser deposition; ALD: Atomic layer deposition; HVPE: Halide vapor phase epitaxy; MOCVD: Metal-organic chemical vapor deposition; MSM: Metal-semiconductor-metal; HRXRD: High-resolution X-ray diffraction; FWHM: Full width at half maximum; AFM: Atomic Force Microscope; RMS: Root-mean-square

Acknowledgements

Not applicable.

Authors' Contributions

HDH and YCL carried out the experiments and drafted the manuscript. GQH, YL, JDY, CZF, YFZ, HL, YBW, YCL, and HDH designed the experiments. GQH helped to revise the manuscript. YH supported the study. All the authors read and approved the final manuscript.

Funding

The authors acknowledge support from the National Key Research and Development Project (grant no. 2018YFB2200500, 2018YFB2202800) and the National Natural Science Foundation of China (grant no. 61534004, 91964202, 61874081, and 61851406).

Availability of Data and Materials

The datasets supporting the conclusions of this article are included within the article.

Competing Interests

The authors declare that they have no competing interests.

Author details

[1]State Key Discipline Laboratory of Wide Band Gap Semiconductor Technology, School of Microelectronics, Xidian University, Xi'an 710071, China. [2]School of Electronic Science and Engineering, Nanjing University, Nanjing 210093, China.

Received: 12 January 2020 Accepted: 14 April 2020
Published online: 07 May 2020

References

1. Itzler M, Donati S, Unlu MS, Kato K (2004) Introduction to the Issue on Photodetectors and Imaging. IEEE Journal of Selected Topics in Quantum Electronics 10:665–667
2. Li W, Zhao X, Zhi Y, Zhang X, Chen Z, Chu X, Yang H, Wu Z, Tang W (2018) Fabrication of cerium-doped β-Ga_2O_3 epitaxial thin films and deep ultraviolet photodetectors. Appl Opt 57:538–543
3. Zhang W, Xu J, Ye W, Li Y, Qi Z, Dai J, Wu Z, Chen C, Yin J, Li J, Jiang H, Fang Y (2015) High-performance AlGaN metal-semiconductor-metal solar-blind ultraviolet photodetectors by localized surface plasmon enhancement. Appl Phys Lett 106:021112
4. Yang W, Hullavarad SS, Nagaraj B, Takeuchi I, Sharma RP, Venkatesan T (2003) Compositionally-tuned epitaxial cubic $Mg_xZn_{1-x}O$ on Si (100) for deep ultraviolet photodetectors. Appl Phys Lett 82:3424–3426
5. Oshima T, Okuno T, Fujita S (2007) Ga_2O_3 thin film growth on c-plane sapphire substrates by molecular beam epitaxy for deep-ultraviolet photodetectors. Japanese Journal of Appl Phys 46:7217
6. Guo D, Wu Z, Li P, An Y, Liu H, Guo X, Yan H, Wang G, Sun C, Li L, Tang WH (2014) Fabrication of β-Ga_2O_3 thin films and solar-blind photodetectors by laser MBE technology. Opt Mat Express 4:1067–1076
7. Kim JK, Lee JM (2016) Electrical and optical properties of near UV transparent conductive ITO/Ga_2O_3 multilayer films deposited by RF magnetron sputtering. Appl Phys Lett 109:172107
8. Seiler W, Selmane M, Abdelouhadi K, Perrière J (2015) Epitaxial growth of gallium oxide films on c-cut sapphire substrate. Thin Solid Films 589:556–562
9. Petitmangin A, Gallas B, Hebert C, Perriere J, Binet L, Barboux P, Portier X (2013) Characterization of oxygen deficient gallium oxide films grown by PLD. Applied Surface Science 278:153–157
10. Comstock DJ, Elam JW (2012) Atomic layer deposition of Ga_2O_3 films using trimethylgallium and ozone. Chemistry of Materials 24:4011–4018
11. Nikolaev VI, Pechnikov AI, Stepanov SI, Nikitina IP, Smirnov AN, Chikiryaka AV, Sharofidinov SS, Bougrov VE, Romanov AE (2016) Epitaxial growth of ($\bar{2}$0 1) β-Ga_2O_3 on (0001) sapphire substrates by halide vapour phase epitaxy. Materials Science in Semiconductor Processing 47:16–19
12. Chen Y, Liang H, Xia X, Shen R, Liu Y, Luo Y, Du G (2015) Effect of growth pressure on the characteristics of β-Ga_2O_3 films grown on GaAs (100) substrates by MOCVD method. Applied Surface Science 325:258–261
13. Li Y, Trinchi A, Wlodarski W, Galatsis K, Kalantar-zadeh K (2003) Investigation of the oxygen gas sensing performance of Ga_2O_3 thin films with different dopants. Sensors and Actuators B: Chemical 93:431–434
14. Higashiwaki M, Sasaki K, Kamimura T, Wong MH, Krishnamurthy D, Kuramata A, Masui T, Yamakoshi S (2013) Depletion-mode Ga_2O_3 metal-oxide-semiconductor field-effect transistors on β-Ga_2O_3 (010) substrates and temperature dependence of their device characteristics. Appl Phys Lett 103:123511
15. Åhman J, Svensson G, Albertsson J (1996) A reinvestigation of β-gallium oxide. Acta Cryst Section C 52:1336–1338
16. Yu F, Yuan DR, Duan XL, Guo SY, Wang XQ, Cheng XF, Kong LM (2008) A simple process to synthesize sphere-shaped gadolinium gallium garnet nanoparticles for transparent ceramic. Journal of Alloys and Compounds 465:567–570
17. Fleischer M, Hanrieder W, Meixner H (1990) Stability of semiconducting gallium oxide thin films. Thin Solid Films 190:93–102
18. Battiston GA, Gerbasi R, Porchia M, Bertoncello R, Caccavale F (1996) Chemical vapour deposition and characterization of gallium oxide thin films. Thin Solid Films 279:115–118
19. Goyal A, Yadav BS, Thakur OP, Kapoor AK, Muralidharan R (2014) Effect of annealing on β-Ga_2O_3 film grown by pulsed laser deposition technique. Journal of Alloys and Compounds 583:214–219
20. Kranert C, Jenderka M, Lenzner J, Lorenz M (2015) Lattice parameters and Raman-active phonon modes of β-$(Al_xGa_{1-x})_2O_3$. Journal of Applied Physics 117:125703
21. Li J, Chen X, Ma T, Cui X, Ren F, Gu S, Zhang R, Zheng Y, Ringer SP, Fu L, Tan HH, Jagadish C, Ye J (2018) Identification and modulation of electronic band structures of single-phase β-$(Al_xGa_{1-x})_2O_3$ alloys grown by laser molecular beam epitaxy. Appl Phys Lett 113:041901
22. Peelaers H, Varley JB, Speck JS, Van de Walle CG (2018) Structural and electronic properties of Ga_2O_3-Al_2O_3 alloys. Appl Phys Lett 112:242101
23. Gullapalli SK, Vemuri RS, Ramana CV (2010) Structural transformation induced changes in the optical properties of nanocrystalline tungsten oxide thin films. Appl Phys Lett 96:171903
24. Subrahmanyam A, Karuppasamy A (2007) Optical and electrochromic properties of oxygen sputtered tungsten oxide (WO_3) thin films. Solar energy materials and solar cells 91:266–274
25. Yu F, Ou S, Wuu D (2015) Pulsed laser deposition of gallium oxide films for high performance solar-blind photodetectors. Opt Mat Express 5:1240–1249
26. Shen H, Yin Y, Tian K, Baskaran K, Duan L, Zhao X, Tiwari A (2018) Growth and characterization of β-Ga_2O_3 thin films by sol-gel method for fast-response solar-blind ultraviolet photodetectors. Journal of Alloys and Compounds 766:601–608
27. Hu GC, Shan CX, Zhang N, Jiang MM, Wang SP, Shen DZ (2015) High gain Ga_2O_3 solar-blind photodetectors realized via a carrier multiplication process. Opt express 23:13554–13561
28. Guo DY, Wu ZP, An YH, Guo XC, Chu XL, Sun CL, Li LH, Li PG, Tang WH (2014) Oxygen vacancy tuned Ohmic-Schottky conversion for enhanced performance in β-Ga_2O_3 solar-blind ultraviolet photodetectors. Appl Phys Lett 105:023507
29. Liu N, Fang G, Zeng W, Zhou H, Cheng F, Zheng Q, Yuan L, Zou X, Zhao X (2010) Direct growth of lateral ZnO nanorod UV photodetectors with Schottky contact by a single-step hydrothermal reaction. ACS Appl Mater Interfaces 2:1973–1979
30. Wang J, Ye L, Wang X, Zhang H, Li L, Kong C, Li W (2019) High transmittance β-Ga_2O_3 thin films deposited by magnetron sputtering and

post-annealing for solar-blind ultraviolet photodetector. Journal of Alloys and Compounds 803:9–15
31. Pratiyush AS, Krishnamoorthy S, Solanke SV, Xia Z, Muralidharan R, Rajan S, Nath DN (2017) High responsivity in molecular beam epitaxy grown β-Ga_2O_3 metal semiconductor metal solar blind deep-UV photodetector. Appl Phys Lett 110:221107
32. Zhang D, Zheng W, Lin RC, Li TT, Zhang ZJ, Huang F (2018) High quality β-Ga_2O_3 film grown with N_2O for high sensitivity solar-blind-ultraviolet photodetector with fast response speed. Journal of Alloys and Compounds 735:150–154
33. Hou X, Sun H, Long S, Tompa GS, Salagaj T, Qin Y, Zhang Z, Tan P, Yu S, Liu M (2019) Ultrahigh-performance solar-blind photodetector based on α-phase-dominated Ga_2O_3 film with record low dark current of 81 fA. IEEE Electron Device Letters 40:1483–1486
34. Pavesi M, Fabbri F, Boschi F, Piacentini G, Baraldi A, Bosi M, Gombia E, Parisini A, Fornari R (2018) ε-Ga_2O_3 epilayers as a material for solar-blind UV photodetectors. Materials Chemistry and Physics 205:502–507

Publisher's Note